SCIENTIFIC REPORTS

OPEN

SUBJECT AREAS:
SUPERCONTINUUM GENERATION
LASER-PRODUCED PLASMAS
NONLINEAR OPTICS
ULTRAFAST PHOTONICS

Received
29 July 2014

Accepted
5 November 2014

Published
1 December 2014

Correspondence and requests for materials should be addressed to M.R. (mcr@creol.ucf.edu)

Transition from linear- to nonlinear-focusing regime in filamentation

Khan Lim, Magali Durand, Matthieu Baudelet & Martin Richardson

Laser Plasma Laboratory, Townes Laser Institute, College of Optics and Photonics, University of Central Florida, Orlando, FL 32816, USA.

Laser filamentation in gases is often carried out in the laboratory with focusing optics to better stabilize the filament, whereas real-world applications of filaments frequently involve collimated or near-collimated beams. It is well documented that geometrical focusing can alter the properties of laser filaments and, consequently, a transition between a collimated and a strongly focused filament is expected. Nevertheless, this transition point has not been identified. Here, we propose an analytical method to determine the transition, and show that it corresponds to an actual shift in the balance of physical mechanisms governing filamentation. In high-NA conditions, filamentation is primarily governed by geometrical focusing and plasma effects, while the Kerr nonlinearity plays a more significant role as NA decreases. We find the transition between the two regimes to be relatively insensitive to the intrinsic laser parameters, and our analysis agrees well with a wide range of parameters found in published literature.

Laser filamentation in gases has been an active area of research for the past two decades[1–3]. Thanks to the many unique properties of laser filaments, a wide range of potential applications have been proposed and demonstrated. Some applications, such as guiding microwaves[4], lightning protection[5] and triggering rain and snow[6], have obvious real-world impact. Others, such as the generation of terahertz radiation[7], the generation of few-cycle ultrashort pulses[8] and the "air-laser"[9], are subtler but no less important to the scientific community and the development of new technologies.

Laser filaments form as a result of a dynamic balance that exists between linear and nonlinear propagation effects. When an ultrashort laser pulse propagating in air has a peak power exceeding the critical power for self-focusing (typically in the range of 3–10 GW for 800 nm), the self-induced index gradient due to the optical Kerr effect causes the beam to focus. Once the focusing beam reaches a high enough intensity (few 10^{13} W/cm^2), photo-ionization of the air occurs and a plasma channel begins to form, and the negative index contribution of the free electrons serves to defocus the beam. The balance between diffraction, Kerr-induced self-focusing (KSF) and plasma defocusing allows the pulse to propagate as a highly confined beam of ~100 μm (FWHM) diameter for distances significantly longer than the Rayleigh length. The pulse leaves behind a plasma channel with a plasma density ~10^{16} cm^{-3}, and its original spectrum can be broadened during filamentation to a supercontinuum spanning multiple octaves from the ultraviolet into the infrared (IR)[2].

In studies conducted over the past two decades, filaments have been formed in very diverse conditions. Experiments in the field are often carried out with large laser systems, sometimes coupled to weakly focusing telescopes, creating filaments over hundreds of meters at a range of few kilometers in the atmosphere[10–13]. On the other hand, filaments in the laboratory are typically generated from smaller beams that are focused at more moderate distances of a few meters[1,14–16], both due to space constrains as well as for better filament stability. The effect of geometrical focusing on filamentation has been previously reported. It has been demonstrated that tighter focusing, high numerical aperture (NA) conditions will lead to higher plasma densities[17–21], and that the spectrum of a tightly focused 800 nm pulse broadens towards the visible but not the IR[22–24]. Even though these differences have been explained by the dominance of geometrical focusing over KSF and plasma defocusing, the transition point where geometrical focusing becomes dominant in filamentation has not been well defined, and the effect of geometrical focusing on the dynamic balance of linear and nonlinear effects in the filament has not been thoroughly investigated.

In any given condition, a filament's properties can be difficult to predict due to the complex physical processes involved; lengthy numerical simulations are often required. Marburger's formula[25] stands out as an analytical tool

which provides the theoretical collapse position of a self-focusing beam, and therefore a good approximation of the position where filamentation begins. In this article, we propose an additional analytical tool that defines the physical regime in which filamentation occurs. Using both numerical and experimental results, the method is validated and the importance of the Kerr effect is shown to diminish in filaments from high-NA beams. Using this analytical method, we investigate the dependence of the transition point between regimes on common experimental parameters, and verify our findings with past results reported by various research groups.

Results

Analytical determination of the transition point. Filamentation in gases is primarily governed by diffraction, KSF and plasma defocusing. Other effects such as multi-photon absorption, plasma absorption and dispersion contribute, but are typically not critical in defining the key characteristics of a filament. In the initial analysis carried out by Braun *et al.*[1], the effects of plasma defocusing and diffraction were assumed to be in static equilibrium with that of KSF in a filament. Despite being a highly simplified description of the filamentation process, the analysis yielded values of intensity and plasma density in a filament that are representative of values found subsequently, both experimentally and numerically. This approach can be adapted for a geometrically focused beam by replacing the diffraction term with one describing the focusing effects of a Gaussian beam.

Figure 1a illustrates how the wavefront sag of a focusing Gaussian beam is calculated for any longitudinal position. For a Gaussian beam, the $1/e^2$ beam radius and the radius of curvature of the wavefront at any position z is given by $w(z) = w_0\sqrt{1+((z-f)/z_R)^2}$ and $R(z) = (z-f)(1 + (z_R/(z-f))^2)$ respectively, where w_0 is the radius of the beam waist, $z = f$ is the position of the geometrical focus and $z_R = \pi w_0^2/\lambda_0$ is the Rayleigh distance. The sag contributed by Kerr and plasma effects can be approximated by the accumulated optical path length difference between the center and the edge of the beam, $s = -\int_0^z \Delta n(z')dz'$. For the Kerr effect, $\Delta n(z) = n_2 I_0(z)$ where n_2 is the nonlinear refractive index of the propagation medium and I_0 is the on-axis intensity. For plasma defocusing, $\Delta n(z) = -\rho(z)/2\rho_c$ where ρ is the on-axis plasma density and ρ_c is the critical plasma density. As the contributions from Kerr and plasma effects are small compared to that of geometrical optics at the initial stage, the intensity can be approximated by $I_0(z) = 2P_0/\pi w(z)^2$, where P_0 is the peak power of the pulse. For laser intensities in a filament, the ionization rate of gases is fairly well approximated by the multi-photon ionization (MPI) rate[26], and the plasma density can be approximated by $\rho(z) = \sigma_K \rho_{nt} \tau (I_0(z))^K$ for the purpose of this analysis, where σ_k is the MPI cross-section, ρ_{nt} the density of neutrals, τ the pulse duration and K the number of photons required to overcome the ionization potential. The sag from geometrical focusing, KSF and plasma defocusing can therefore be expressed respectively as

$$s_G = \frac{w_0^2}{2z_R^2}(z-f) \tag{1}$$

$$s_K = \frac{2n_2 P_0 z_R}{\pi w_0^2}\left(\tan^{-1}\frac{z-f}{z_R} + \tan^{-1}\frac{f}{z_R}\right) \tag{2}$$

$$s_p = \frac{\sigma_K \rho_{nt} \tau z_R}{2\rho_c}\left(\frac{2P_0}{\pi w_0^2}\right)^K \frac{(2K-2)!}{(2^{K-1}(K-1)!)^2}\left(h_K\left(\frac{z-f}{z_R}\right) + h_K\left(\frac{f}{z_R}\right)\right) \tag{3}$$

where

$$h_K(x) = \tan^{-1} x + \sum_{n=1}^{K-1} \frac{(2^n n!)^2}{(2n)!}\frac{x}{2n(1+x^2)^n} \tag{4}$$

When the beam is far from the geometrical focus and the intensity is low, the nonlinear effects are weak and $|s_G|$ is significantly larger than $|s_K|$ and $|s_p|$. As the intensity increases near the focus, $|s_K|$ and $|s_p|$ can increase rapidly. We define the position z_K as the position where $|s_K| = |s_G|$, when KSF becomes non-negligible compared to geometrical focusing. The position z_p is similarly defined for plasma defocusing ($|s_p| = |s_G|$).

Figure 1b–d shows the calculations for three different focal conditions. The initial parameters of the pulse are $w(0) = 4.25$ mm, $\tau = 50$ fs, $\lambda_0 = 800$ nm and pulse energy $E = 0.8$ mJ. The peak power is calculated by $P_0 = \sqrt{4\ (\ln\ 2)/\pi}(E/\tau)$. Based on the PPT model for photoionization, the ionization rate of oxygen is three orders of magnitude greater than that of nitrogen[26] for excitation at 800 nm and intensities $\sim 10^{13}$ Wcm^{-2}. It is therefore reasonable to neglect the contribution of nitrogen relative to oxygen when calculating plasma densities[2,27]. For ionization of oxygen (ionization potential $U_O = 12.1$ eV), the MPI parameters used for this analysis are $K = 8$, $\sigma_K = 2.81 \times 10^{-96}$ W^{-8}cm^{16}s^{-1} and $\rho_{nt} = 0.54 \times 10^{19}$cm^{-3}. The nonlinear refractive index and critical plasma density are $n_2 = 3 \times$

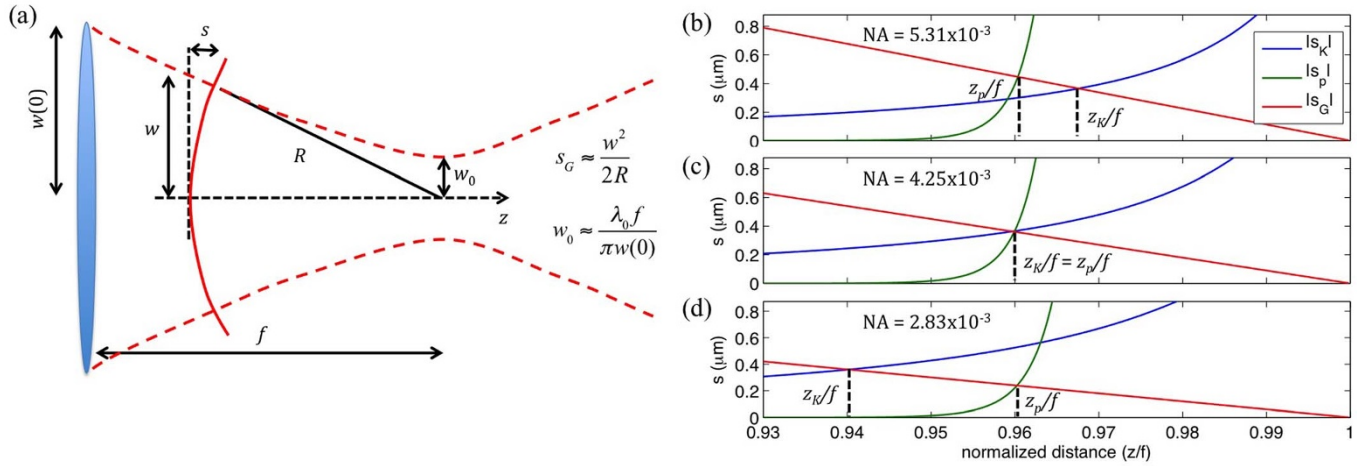

Figure 1 | Analysis of wavefront sag induced by Gaussian beam focusing, KSF and plasma defocusing. (a) Illustration of wavefront sag for a focusing Gaussian beam. (b,c,d) Calculations of wavefront sag contribution by KSF (s_K), plasma defocusing (s_p) and geometrical focusing (s_G) for focusing conditions NA = 5.31×10^{-3}, 4.25×10^{-3} and 2.83×10^{-3} respectively. The positions z_K and z_p, where the sag contribution from KSF and plasma defocusing become more significant than that from geometrical focusing, are indicated.

10^{-19} $W^{-1}cm^2$ and $\rho_c = 1.7 \times 10^{21}$ cm^{-3}. In high-NA conditions, geometrical focusing is more significant and the Kerr effect has less propagation distance to build up. In low-NA conditions, the opposite is true. The onset of plasma defocusing is much more sudden once the intensity builds up to $> 10^{13}$ Wcm^{-2}, regardless of geometrical focusing conditions. As a result, $z_K > z_p$ in high-NA conditions while $z_K < z_p$ in low-NA conditions. We can therefore define the geometrical focusing condition where $z_K = z_p$ as the transition between high- and low-NA regimes for filamentation. Using our initial beam parameters, this transition occurs at the numerical aperture $NA_T = 4.28 \times 10^{-3}$ ($f = 0.99$ m), defined as the ratio between $w(0)$ and the geometrical focal distance (Figure 1c). Note that a numerical simulation was not required to obtain this result, allowing different initial conditions to be analyzed rapidly.

Numerical and experimental verification. To verify that the proposed analytical method accurately determines the transition between focusing regimes, a series of numerical simulations were carried out. The same initial beam parameters as those in Figure 1 were used, and the beam was initially focused at different conditions varying from NA = 0.85×10^{-3} ($f = 5$ m) to 11×10^{-3} ($f = 0.4$ m). To evaluate the relative importance of KSF and plasma defocusing, the same simulations were repeated, but with the terms describing Kerr effect or plasma effects removed. Some of the results are shown in Figure 2. In the left column, the beam sizes from the different simulations are plotted together for comparison. The positions of z_K, z_p and the theoretical collapse position predicted by Marburger's formula[25] are also indicated in the plots. By comparing the beam sizes for linear focusing (black dotted lines) against the results without Kerr effect (red dash-dot lines), the location where plasma defocusing becomes important, assuming the absence of Kerr effect, can be easily determined. This position corresponds well to z_p. This substantiates our definition of z_p. The definition of z_K is also consistent with the simulations, as it occurs before the theoretical collapse of the beam; KSF must become prominent before beam collapse takes place.

To evaluate whether $z_K = z_p$ accurately describes the transition point between high- and low-NA conditions, we examine the differences in the two regimes defined by this transition. In the high-NA regime, NA $> 4.28 \times 10^{-3}$ in this case, geometrical focusing and

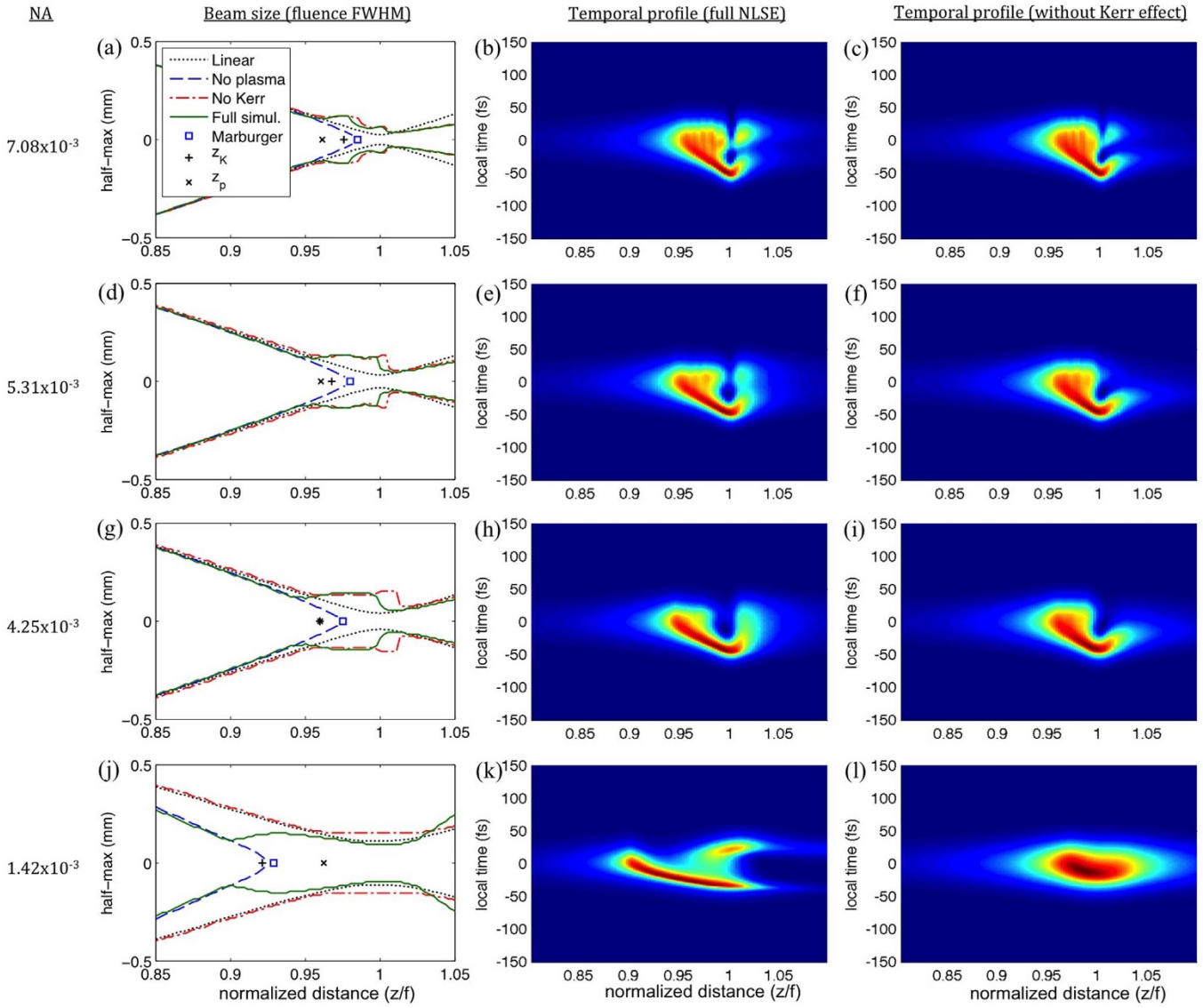

Figure 2 | Simulation of a filamenting beam with different initial focusing conditions. Left column (a,d,g,j) shows the beam sizes (fluence FWHM) derived from different versions of the simulation, as well as the positions of z_K, z_p and the theoretical collapse position of the beams as predicted by Marburger's formula. Center column (b,e,h,k) shows the on-axis temporal profiles of the pulse derived from the full NLSE, while the right column (c,f,i,l) shows the temporal profiles when the simulation is performed without the terms describing the Kerr effect.

plasma defocusing are the primary contributors to the filamentation process, while KSF plays a noticeable but secondary role. From Figure 2a–f, it is clear that the beam size and the temporal profiles from the full simulation and the simulation without Kerr effect bear strong similarities. This similarity quickly disappears for lower NA (Figure 2g–l). Without a sufficient propagation distance for KSF to build up, geometrical focusing dominates for most of the distance as the beam converges. Figure 3a shows that, for high-NA, the intensity before the filamentation increases at approximately the same rate over the normalized distance z/f, which is a trend consistent with geometrical focusing. When the intensity increases beyond 10^{13} Wcm^{-2}, the plasma density increases rapidly (Figure 3b), significantly slowing or arresting further focusing, and filamentation begins. This occurs at approximately the same normalized distance, and z_p provides a better approximation of this distance compared to Marburger's formula (Figure 3c). With strong geometrical focusing, the plasma densities are significantly higher than the typical value of a few 10^{16} cm^{-3}.

In the low-NA regime, KSF has sufficient distance to build up and eventually dominate over geometrical focusing. The intensity of the pulse therefore increases more rapidly than in linear propagation, and the filament is formed further from the geometrical focal point. Filaments formed in low-NA conditions exhibit characteristics that are typically described – a clamped intensity value of $\sim 3 \times 10^{13}$ Wcm^{-2}, plasma densities between $2–3\times10^{16}$ cm^{-3}, and the position where filamentation begins approximately follows Marburger's formula (Figure 3). A behavior that is present in the low-NA but not the high-NA regime is pulse splitting. As plasma is mostly formed near the peak of the pulse, plasma defocusing affects primarily energy at the rear of the pulse. With enough distance, KSF refocuses the energy to form a second pulse behind the first pulse; this behavior is seen in Figure 3k, and has been previously observed in air[14,28]. Pulse splitting is therefore a clear indicator that KSF plays a critical role in the low-NA regime.

To better identify filamentation in high-NA and low-NA conditions with the dominant focusing mechanism governing the filamentation process, the regimes can also be called the linear-focusing regime and the nonlinear-focusing regime respectively. Due to the different dominant physical mechanisms in the two regimes, the supercontinuum generated by filamentation is markedly different[2,23]. When the Kerr effect is significant, spectral broadening due to self-phase modulation expands the original spectrum on both sides. Spectral broadening due to plasma effect occurs primarily towards the high frequencies, as the pulse experiences a rapid reduction in the effective index of refraction while plasma is created. In the linear-focusing regime (Figure 4a), broadening in the IR is minimal and does not vary with geometrical focusing, while broadening in the visible decreases as the focusing condition approaches the transition at $NA = NA_T = 4.28\times10^{-3}$. Beyond this point (Figure 4b), broadening in the IR increases with decreasing NA, while broadening in the visible also increases after a slight initial decrease. The results are replicated experimentally, with initial conditions $w(0) = 4.25$ mm, $\tau = 50$ fs, and pulse energy $E = 3$ mJ, and are shown in Figure 4e and f. Observation of spectral broadening is therefore the most convenient experimental method to determine which regime is dominant. It also allows one to estimate its proximity to the transition point.

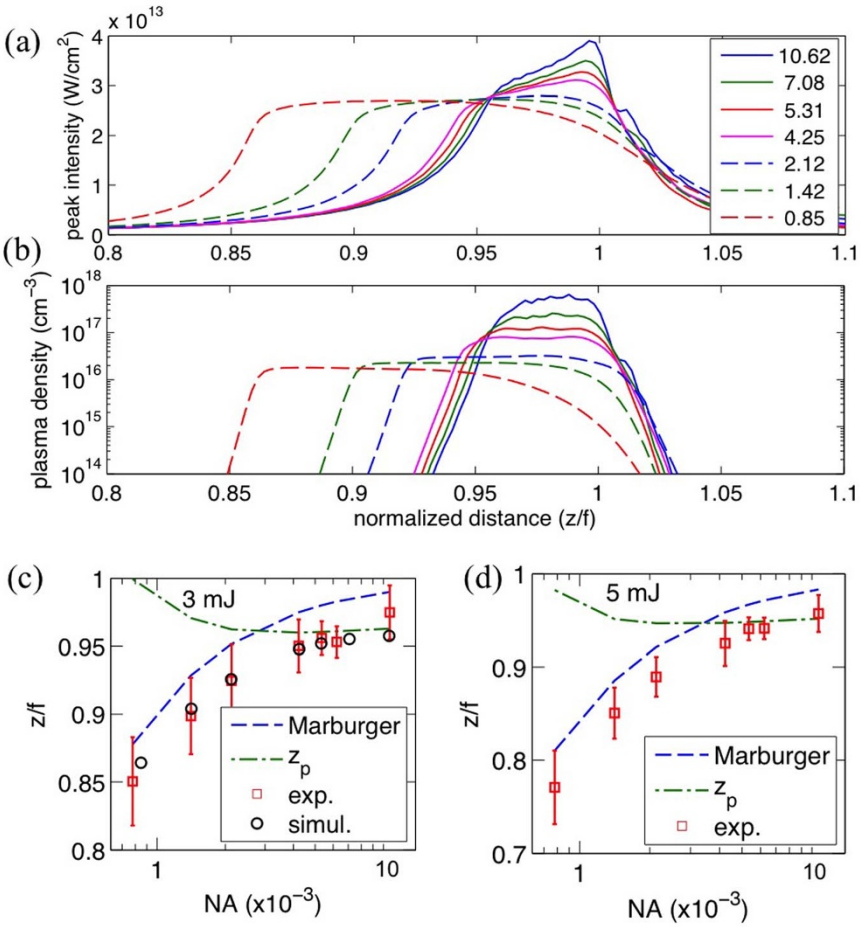

Figure 3 | Plots of filament intensity, plasma density and position where filamentation begins. (a,b) Numerically derived intensity and plasma density of filaments with different initial focusing conditions (indicated in NAx10^3 by the legend). (c,d) Position where filamentation begins, comparing experimental observations with simulation results and calculated values of z_K and z_p.

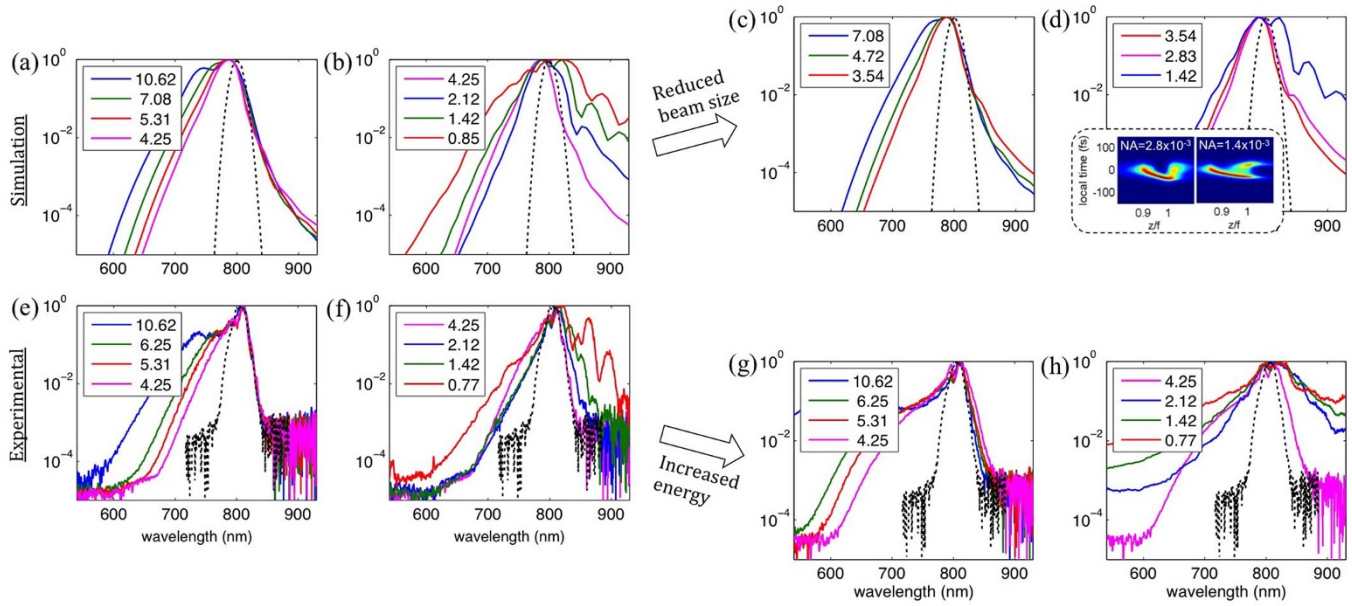

Figure 4 | Spectra of supercontinuum after filamentation, with different initial focal conditions (NAx10^3) indicated in legends. (a,b) Simulation results with initial beam parameters $w(0) = 4.25$ mm, $\tau = 50$ fs and $E = 0.8$ mJ. (c,d) Same as (a,b) except $w(0) = 2.83$ mm. Inset in (d) shows the temporal profile of the pulse for NA $= 2.8 \times 10^{-3}$ and NA $= 1.4 \times 10^{-3}$. (e,f) Measured spectra with initial beam parameters $w(0) = 4.25$ mm, $\tau = 50$ fs and $E = 3$ mJ. (g,h) Same as (e,f) except $E = 16$ mJ. The black dotted line in each plot represents the initial spectrum of the pulse.

Generalization of the results. In the results presented up to this point, the geometrical focusing condition has been the only variable. The calculation of z_K and z_p can be carried out with a wider range of initial conditions to determine the effect of other parameters on the transition between linear-focusing and nonlinear-focusing regimes. We varied three different parameters, the initial beam size, the pulse duration and the peak power, within ranges that are representative of values used in experimental settings. s_G, s_K and s_p were recalculated for each set of parameters for different focusing conditions until NA_T, the focusing condition where $z_K = z_p$, was found. The results shown in Figure 5 indicate that despite significant, order-of-magnitude changes in all three beam parameters, variations of NA_T are relatively small. This implies that the balance between the focusing and defocusing mechanisms is most strongly determined by the geometrical focusing condition alone. In fact, for longer pulses ($\tau > 100$ fs), the delayed Raman Kerr

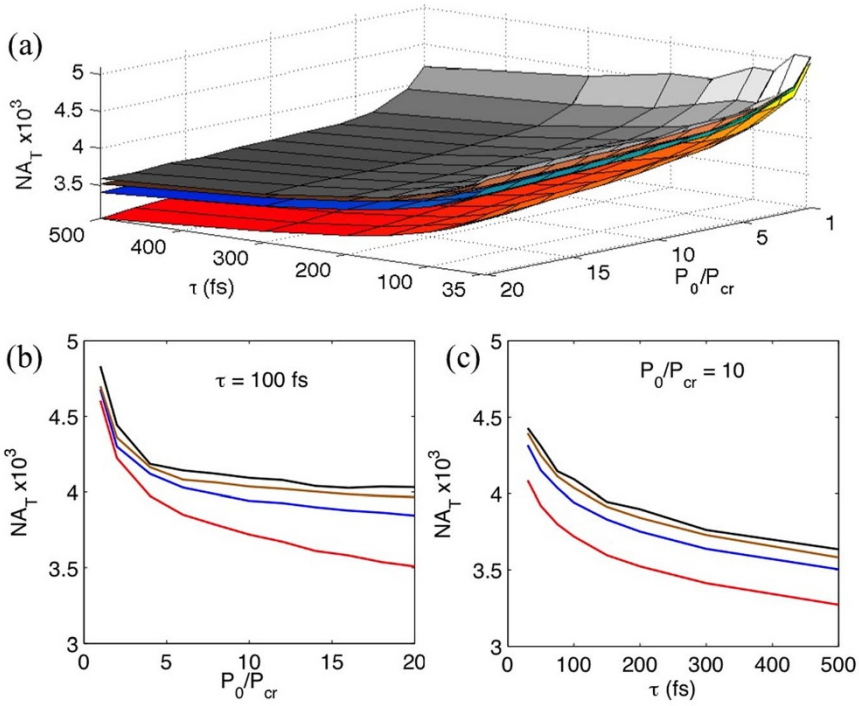

Figure 5 | Evolution of NA_T with common parameters. (a) Values of NA_T for different initial beam size, pulse duration and peak power. Surfaces in red, blue, brown and gray represent data for initial FWHM beam diameters of 2 mm, 5 mm, 10 mm and 20 mm respectively. (b,c) Cross-sections of the surfaces in (a) for pulse duration of 100 fs and $P_0 = 10P_{cr}$.

Table 1 | Analysis of focusing regime applied to previously published results of filamentation at 800 nm. Left column displays experimental or simulation conditions, right column describes analysis and supporting evidence. Bottom section includes analysis of filamentation in argon

Ref.	Med.	E (mJ)	τ (fs)	w(0) (mm)	f (m)	NA x10^3	NA_T x10^3	Regime	Remarks and evidence
32	air	0.5–5	35–200	12.5	0.1	125	3.9–4.7	linear	Plasma density $> 10^{18}$ cm^{-3}
23	air	2.4–47	60	15	0.13	118	1.9–4.2	linear	Strong broadening in visible, none in IR
14	air	0.7	100	2	1.5	1.3	4.2	non-linear	Broadening in both directions, pulse splitting, plasma density $\sim 10^{16}$ cm^{-3}
33	air	1	30	3	1–4	0.75–3	4.3	non-linear	Broadening in both directions (consider only non-HOKE case)
34	air	60	115	21	8	2.7	3.2	non-linear	Broadening in the IR, high energy compensates for being close to NA_T
17	air	$10P_{cr}$	100	1		0.1–10	3.5	both	Change in trends between NA = 0.002 and 0.004, beam size deviate from linear focusing for NA < 0.002
18	air	Data compiled from various conditions, includes ref. 19					~3.9	both	Change in trends between NA = 0.003 and 0.006
16	air	Range of conditions					3.4–3.9	both	Appearance (NA 0.0037) and strengthening (NA 0.0013) of refocusing events
35	Ar 1atm	1	35	3.8	2.4	1.6	5.9	non-linear	Strong broadening in both directions
15	Ar 0.9atm	0.66	30	5.3	1	5.3	5.8	non-linear	Broadening in both directions
36	Ar 0.5atm	4.5	45	8.9	1.5	5.9	4.1	linear	Strong broadening in visible, very weak broadening in IR

effect, which has not been taken into consideration in the determination of NA_T, should lead to stronger self-focusing. Having an effectively stronger Kerr effect would lead to $|s_K|$ increasing more rapidly with propagation. This would result in higher effective NA_T values for long pulses, and therefore less variation of NA_T with pulse duration.

The relative invariance of NA_T can be explained by the dependence of both the Kerr and plasma effects on intensity. For conditions close to the transition point, the propagation of the beam prior to filamentation resembles that of a Gaussian beam. Typical initial intensities are in the range of 10^{10}–10^{11} W/cm^2, which is a few orders of magnitude lower than that in a filament, and increases approximately as $1/(z-f)^2$ towards the geometrical focus; i.e. intensity increases slowly initially and much more rapidly near the geometrical focus. For the focusing conditions under consideration, the build-up of the Kerr effect, as represented by the rate of increase of $|s_K|$, is most significant at intensities $> 10^{12}$ W/cm^2. The build-up of plasma, $|s_p|$, is strongly intensity dependent and increases sharply at intensities around 10^{13} W/cm^2. The Kerr and plasma effects are therefore only felt close to the geometrical focus. Together with the approximate $1/(z-f)^2$ dependence of the intensity, this implies that changes in the initial beam parameters only cause a relatively small change in the positions z_K and z_p. As a result, a small change in the focusing condition is sufficient to compensate for comparatively large changes in the initial beam parameters.

To verify the relative invariance of NA_T, additional measurements and simulations were performed. In Figure 4g and h, the spectrum after filamentation was measured with the pulse energy increased to 16 mJ. A recalculation of NA_T for the higher energy pulses show a slight decrease of its value from 4.28×10^{-3} to 4.01×10^{-3}. The same spectral broadening trends can be observed as in Figure 4e and f, showing that the transition can still be observed spectrally for increased pulse energies. Additional simulations were carried out with a smaller initial beam ($w(0)$=2.83 mm) while maintaining the same pulse duration and energy, and the spectral results plotted in Figure 4c and d. For the smaller beam, NA_T is calculated to be 4.25×10^{-3}. The spectral broadening trend is similar, but not as pronounced as for the larger beam. Broadening in the IR is present but weak for NA = 3.54×10^{-3} and 2.83×10^{-3}, and only becomes strong at NA = 1.42×10^{-3}. By examining the temporal profiles for NA = 2.83×10^{-3} and 1.42×10^{-3} (inset, Figure 4d), it can be seen that the filament length for NA = 2.83×10^{-3} is insufficient for pulse splitting to develop. It has been demonstrated for filamentation in water that a strong correlation exists between pulse splitting and spectral broadening[29]. A similar correlation exists here, demonstrating the universality of the physics governing filamentation across different media.

Discussion

Knowing and understanding the transition between linear-focusing and nonlinear-focusing regimes that govern filamentation can be important for research into applications of filamentation. Due to space constraints in the laboratory, it may not always be possible to work with filaments from collimated beams. In addition, geometrical focusing can help to stabilize the transverse and longitudinal position of the filaments and render results more repeatable on a shot-to-shot basis. However, if the focusing conditions are too close to the transition between focusing regimes, the balance between the physical mechanisms may be undesirably skewed. Depending on the properties of the filament being investigated, it is possible that the results demonstrated in one regime may not be directly applicable in the other regime. For example, experiments carried out in the non-linear-focusing regime would have greater relevance to long-distance propagation applications. For supercontinuum-related applications, the difference in the primary nonlinear effect contributing to spectral broadening could also make one regime preferable over the other.

It is instructive to investigate the experimental and simulation conditions under which prior research on filamentation has been conducted, and to determine if the observations made correspond to the focusing regimes proposed in this paper. Initial beam conditions from several published results are presented in Table 1, together with the analysis determining the corresponding focusing regime and reported evidence that support the analysis. The results of Geints *et al.*[17,18] and Talebpour *et al.*[16] are of notable interest, as they straddle a range of conditions where transition effects could be observed. Geints *et al.* reported on the evolution of filament length and plasma density with NA, and a sharp change in the trends could be observed for values of NA in the vicinity of NA_T. Talebpour *et al.*

reported observing refocusing events, which is an indicator of KSF at work, when $NA \leq NA_T$ but not for larger NA. To demonstrate that the focusing regime analysis can be applied to gases other than air, published results of filamentation in argon were also examined. For the examples of filamentation in argon cited in Table 1, the values of NA_T were calculated using the parameters given in Reference 8. The reported spectral broadening in these examples agree well with the focusing regimes in which the filaments are formed, as determined by the corresponding values of NA_T.

The calculation of the sag contributions s_K and s_p assumes that the beam remains comparable to a linearly focusing Gaussian beam. In such a situation, z_K and z_p would be located relatively near to the geometrical focal point. Examples of conditions where the values of s_K and s_p may no longer be meaningful are high-NA pulses with high energy, where small-scale filamentation[21] or "superfilamentation"[30] takes place, and very low-NA beams, where KSF changes the beam focusing dynamics significantly from that of the linear case. Two approximations are made in the formulation of equations (1–3). The first, $w_0 \approx \lambda_0 f/\pi w(0) = \lambda_0/\pi NA$, is valid in the case where $NA \cdot w(0) \gg \lambda_0/\pi$. The second, $s_G \approx w(z)^2/2R(z)$, is valid when $\lambda_0/\pi w_0 \ll 1$, i.e. $NA \ll 1$. For the analysis of transition between regimes, it is important that these conditions are fulfilled for $NA \approx NA_T$. The first condition is fulfilled for $\lambda_0 = 800$ nm for typical beam sizes considered, $w(0) > 1$ mm. The second is fulfilled as NA_T has been shown to stay within the range 0.003–0.005.

The analysis presented is based only on the geometrical focusing, KSF and plasma defocusing effects, which is generally applicable for filamentation in gases at near IR wavelengths. To treat filamentation in condensed media, at other wavelengths, or of few-cycle pulses, other effects such as dispersion and losses due to multi-photon absorption and plasma absorption may play more significant roles and need to be taken into consideration. As a result, the physical regimes under consideration and the transition between them may be significantly different from those discussed here.

Conclusions

In summary, we have developed a fully analytical method to classify filamentation in gases of a geometrically focusing beam as being in the linear-focusing (high-NA) or nonlinear-focusing (low-NA) regime. By analyzing filaments formed over a large range of initial beam conditions and by comparing the results published in the literature, we conclude that, for filaments at 800 nm in air, the transition between linear- and nonlinear-focusing regimes typically fall between NA values of 0.003 and 0.005. Our results demonstrate a clear difference in the active physical mechanisms involved when moving from one regime to the other. The role of KSF diminishes in high-NA conditions, and filamentation becomes primarily governed by geometrical focusing and plasma effects.

Methods

Marburger's formula. The theoretical collapse position of an initially collimated beam undergoing KSF is given by

$$z_{sf} = \frac{0.367\pi n_0 w(0)^2/\lambda_0}{\sqrt{\left(\sqrt{P_0/P_{cr}} - 0.852\right)^2 - 0.0219}} \tag{5}$$

where the critical power for self-focusing for a Gaussian beam is $P_{cr} = 3.77\lambda_0^2/8\pi n_0 n_2$. For a geometrically focused beam with focal distance f, the modified collapse position z'_{sf} is shifted according to

$$\frac{1}{z'_{sf}} = \frac{1}{z_{sf}} + \frac{1}{f} \tag{6}$$

Numerical simulations of filamentation. Simulations of a pulse undergoing filamentation were carried out by numerically solving the nonlinear Schrödinger equation (NLSE) using the split-step Fourier method. The full NLSE equation used is

$$\begin{aligned}\frac{\partial \varepsilon}{\partial z} = {} & \frac{i}{2n_0k_0}\nabla_\perp^2\varepsilon - i\frac{k''}{2}\frac{\partial^2\varepsilon}{\partial t^2} + ik_0n_2(1-\alpha)|\varepsilon|^2\varepsilon \\ & + ik_0n_2\alpha\left[\int_{-\infty}^{t} R(t-t')|\varepsilon(t')|^2dt'\right]\varepsilon \\ & - \frac{\sigma}{2}(1+i\omega_0\tau_c)\rho\varepsilon \\ & - \frac{\beta_K}{2}|\varepsilon|^{2K-2}\left(1-\frac{\rho}{\rho_{nt}}\right)\varepsilon\end{aligned} \tag{7}$$

where the terms on the right-hand side represent the effects of diffraction, dispersion, electronic Kerr effect, Raman Kerr effect, plasma absorption and defocusing, and MPI losses respectively. $R(t) = R_0\exp(-\Gamma t)\sin(\omega_R t)$ is a function that describes the molecular response of the medium, with $R_0 = \left(\Gamma^2 + \omega_R^2\right)/\omega_R$, Γ^{-1} being the molecular response time and ω_R the molecular rotational frequency. The electric field ε is defined such that the intensity of the beam is given by $I = |\varepsilon|^2$. For simulations in air, the parameters used (from reference 2) are $k'' = 0.2$ fs^2 cm^{-1}, $n_2 = 3 \times 10^{-19}$ W^{-1}cm^2, $\Gamma = 1/70$ fs and $\omega_R = 16 \times 10^{12}$ s^{-1}. The repartitioning factor α between the instantaneous electronic and the delayed molecular Raman Kerr effects is taken to be 0.5. $\tau_c = 350$ fs is the electron collision time, $\sigma \approx 1/(n_0\rho_c c\tau_c) = 5.6 \times 10^{-20}$ cm^2 is the cross section for inverse Bremsstrahlung and $\rho_c = 1.7 \times 10^{21}$ cm^{-3} is the critical plasma density at 800 nm. The rate that free electrons are generated is given by

$$\frac{\partial \rho}{\partial t} = \sigma_K I^K(\rho_{nt} - \rho) + \frac{\sigma}{U_i}\rho I \tag{8}$$

O_2 is assumed to be the main species that is ionized, with ionization potential $U_i = 12.063$ eV and the density of neutrals $\rho_{nt} = 0.54 \times 10^{19}$ cm^{-3}. At 800 nm, 8-photon ionization takes place ($K = 8$) and the ionization cross section is $\sigma_K = 2.81 \times 10^{-96}$ W^{-8}cm^{16}s^{-1}. The MPI coefficient is given by $\beta_K = K\hbar\omega_0\rho_{nt}\sigma_K = 3 \times 10^{-95}$ W^{-7}cm^{13}. To keep computing time and resources manageable, circular symmetry is assumed. To obtain the best agreement with experimental results, the pulse energies used in simulations (as well as the calculation of NA_T) differ from the experimental values by a factor of 0.27. The use of a lower pulse energy in the simulations and calculations can be justified by the fact that the critical power for self-focusing is known to be higher than the theoretical value ($P_{cr} = 3.2$ GW) for pulses shorter than 200 fs[31]. For the pulses use in the measurements described in this paper, filaments were not observed for peak powers lower than $3P_{cr}$.

Measurement of post-filamentation spectra. The spectrum of the pulse after filamentation was measured using two different fiber-coupled spectrometers (Ocean Optics USB2000 in the near IR and HR2000 in the visible) to cover the full spectral range of interest. The post-filament light was diffused off a white screen and coupled into the collecting fiber with a lens. To ensure that light emitted at all angles from the filament was collected, the diffusion spot on the screen was kept small (while ensuring that no optical damage occurred to the screen) and the spectrum was verified to be unchanged by small movements of the collecting fiber and lens. The system was calibrated and the spectra from both spectrometers combined in post-processing with the aid of a tungsten calibration lamp.

Measurement of the positions where filamentation begins. The position where filamentation began was taken to be where plasma emission began to be visible to the dark-adapted eye in a darkened laboratory. Error-bars in the measured normalized distance account for uncertainties in the observed positions as well as uncertainties in the experimentally determined focal lengths of the lenses used.

1. Braun, A. *et al.* Self-channeling of high-peak-power femtosecond laser pulses in air. *Opt. Lett.* **20**, 73 (1995).
2. Couairon, A. & Mysyrowicz, A. Femtosecond filamentation in transparent media. *Phys. Rep.* **441**, 47–189 (2007).
3. Chin, S. L. *et al.* Advances in intense femtosecond laser filamentation in air. *Laser Phys.* **22**, 1–53 (2011).
4. Kudyshev, Z. A., Richardson, M. C. & Litchinitser, N. M. Virtual hyperbolic metamaterials for manipulating radar signals in air. *Nat. Commun.* **4**, 2557 (2013).
5. Kasparian, J. *et al.* Electric events synchronized with laser filaments in thunderclouds. *Opt. Express* **16**, 5757 (2008).
6. Rohwetter, P. *et al.* Laser-induced water condensation in air. *Nat. Photonics* **4**, 451–456 (2010).
7. Roskos, H. G., Thomson, M. D., Kreß, M. & Löffler, T. Broadband THz emission from gas plasmas induced by femtosecond optical pulses: From fundamentals to applications. *Laser Photonics Rev.* **1**, 349–368 (2007).
8. Mysyrowicz, A., Couairon, A. & Keller, U. Self-compression of optical laser pulses by filamentation. *New J. Phys.* **10**, 025023 (2008).
9. Zhang, H. *et al.* Rotational Coherence Encoded in an "Air-Laser" Spectrum of Nitrogen Molecular Ions in an Intense Laser Field. *Phys. Rev. X* **3**, 041009 (2013).
10. Rodriguez, M. *et al.* Kilometer-range nonlinear propagation of femtosecond laser pulses. *Phys. Rev. E* **69**, 036607 (2004).

11. Méchain, G. *et al.* Range of plasma filaments created in air by a multi-terawatt femtosecond laser. *Opt. Commun.* **247**, 171–180 (2005).
12. Durand, M. *et al.* Kilometer range filamentation. *Opt. Express* **21**, 26836 (2013).
13. Eisenmann, S. *et al.* Control of the filamentation distance and pattern in long-range atmospheric propagation. *Opt. Express* **15**, 2779 (2007).
14. Alonso, B., Sola, I. J., Román, J. S., Varela, Ó. & Roso, L. Spatiotemporal evolution of light during propagation in filamentation regime. *J. Opt. Soc. Am. B* **28**, 1807 (2011).
15. Zaïr, A. *et al.* Spatio-temporal characterization of few-cycle pulses obtained by filamentation. *Opt. Express* **15**, 5394 (2007).
16. Talebpour, A., Petit, S. & Chin, S. L. Re-focusing during the propagation of a focused femtosecond Ti:Sapphire laser pulse in air. *Opt. Commun.* **171**, 285–290 (1999).
17. Geints, Y. É. & Zemlyanov, A. A. Self-focusing of a focused femtosecond laser pulse in air. *Appl. Phys. B* **101**, 735–742 (2010).
18. Geints, Y. É. *et al* Peculiarities of filamentation of sharply focused ultrashort laser pulses in air. *J. Exp. Theor. Phys.* **111**, 724–730 (2010).
19. Théberge, F., Liu, W., Simard, P., Becker, A. & Chin, S. L. Plasma density inside a femtosecond laser filament in air: Strong dependence on external focusing. *Phys. Rev. E* **74**, 036406 (2006).
20. Liu, X.-L. *et al.* Tightly focused femtosecond laser pulse in air: from filamentation to breakdown. *Opt. Express* **18**, 26007 (2010).
21. Prem Kiran, P. *et al.* Focal dynamics of multiple filaments: Microscopic imaging and reconstruction. *Phys. Rev. A* **82**, 013805 (2010).
22. Prem Kiran, P. *et al.* Supercontinuum emission from tightly focused femtosecond pulses in air – beyond intensity clamping. in *Proc. SPIE 7728, Nonlinear Opt. Appl. IV* (Eggleton, B. J., Gaeta, A. L. & Broderick, N. G. R.) **7728**, 77281P (2010).
23. Liu, X.-L. *et al.* Broadband supercontinuum generation in air using tightly focused femtosecond laser pulses. *Opt. Lett.* **36**, 3900 (2011).
24. Heins, A. & Guo, C. Spectral investigation of higher-order Kerr effects in a tight-focusing geometry. *Opt. Express* **21**, 29401 (2013).
25. Marburger, J. H. Self-focusing: theory. *Progr. Quantum Electron.* **4**, 35–110 (1975).
26. Couairon, A. *et al.* Infrared femtosecond light filaments in air: simulations and experiments. *J. Opt. Soc. Am. B* **19**, 1117 (2002).
27. Couairon, A. & Bergé, L. Light Filaments in Air for Ultraviolet and Infrared Wavelengths. *Phys. Rev. Lett.* **88**, 135003 (2002).
28. Bernstein, A. C. *et al.* Asymmetric ultra-short pulse splitting measured in air using FROG. *Appl. Phys. B Lasers Opt.* **75**, 119–122 (2002).
29. Jarnac, A. *et al.* Whole life cycle of femtosecond ultraviolet filaments in water. *Phys. Rev. A* **89**, 033809 (2014).
30. Point, G. *et al.* Superfilamentation in Air. *Phys. Rev. Lett.* **112**, 223902 (2014).
31. Liu, W. & Chin, S. L. Direct measurement of the critical power of femtosecond Ti:sapphire laser pulse in air. *Opt. Express* **13**, 5750 (2005).
32. Abdollahpour, D., Suntsov, S., Papazoglou, D. & Tzortzakis, S. Measuring easily electron plasma densities in gases produced by ultrashort lasers and filaments. *Opt. Express* **19**, 16866 (2011).
33. Béjot, P. & Kasparian, J. Conical emission from laser filaments and higher-order Kerr effect in air. *Opt. Lett.* **36**, 4812 (2011).
34. Kasparian, J. *et al.* Infrared extension of the super continuum generated by femtosecond terawatt laser pulses propagating in the atmosphere. *Opt. Lett.* **25**, 1397 (2000).
35. Schulz, E. *et al.* Tracking spectral shapes and temporal dynamics along a femtosecond filament. *Opt. Express* **19**, 19495 (2011).
36. Skupin, S. *et al.* Self-compression by femtosecond pulse filamentation: Experiments versus numerical simulations. *Phys. Rev. E* **74**, 056604 (2006).

Acknowledgments

This work was funded by the Army Research Office/Multidisciplinary University Research Initiative ("Light Filamentation Science" Contract #W911NF1110297) and the State of Florida. K. Lim is funded by DSO National Laboratories, Singapore.

Author contributions

K.L. and M.D. designed and carried out the experiments to study effects of focusing. K.L. wrote the code and carried out the simulations. K.L. and M.B. conceptualized the analytical transition point and carried out the analysis. M.D. and M.R. initiated and guided the project. K.L. prepared the manuscript. All authors contributed to the discussion and revision of the manuscript.

Additional information

Competing financial interests: The authors declare no competing financial interests.

How to cite this article: Lim, K., Durand, M., Baudelet, M. & Richardson, M. Transition from linear- to nonlinear-focusing regime in filamentation. *Sci. Rep.* **4**, 7217; DOI:10.1038/srep07217 (2014).